

Article

# Strengthening versus Softening of Nanotwinned Copper Depending on Prestress and Twin Spacing

Jing Han <sup>1,\*</sup>, Jiapeng Sun <sup>2,\*</sup> , Ying Han <sup>3</sup>, Hua Zhu <sup>1</sup> and Liang Fang <sup>4</sup>

<sup>1</sup> School of Mechanical and Electrical Engineering, China University of Mining and Technology, Xuzhou 221116, China; zhuhua@cumt.edu.cn

<sup>2</sup> College of Mechanics and Materials, Hohai University, Nanjing 210098, China

<sup>3</sup> Key Laboratory of Advanced Structural Materials, Ministry of Education, Changchun University of Technology, Changchun 130012, China; hanying@ccut.edu.cn

<sup>4</sup> State Key Laboratory for Mechanical Behavior of Materials, Xi'an Jiaotong University, Xi'an 710049, China; fangl@xjtu.edu.cn

\* Correspondence: hanjing@cumt.edu.cn (J.H.); sun.jiap@gmail.com (J.S.);  
Tel.: +86-187-515-10158 (J.H.); +86-133-8268-4178 (J.S.)

Received: 7 April 2018; Accepted: 8 May 2018; Published: 11 May 2018



**Abstract:** This paper addressed the prestress- and twin spacing-dependent deformation as well as the hardening-to-softening transition in nanotwinned copper (nt-Cu) using molecular dynamics simulations. The results demonstrated that the hardening-to-softening transition always occurs at any prestress with decreasing twin spacing in nt-Cu compared with its single crystal counterpart, while it occurs at specific twin spacing with decreasing prestress. The hardening-to-softening transition induced by decreasing twin spacing or prestress is due to the same mechanism, i.e., transition in the initial plasticity mechanism from the activity of partial dislocation to twinning dislocation. Moreover, the indentation hardness increases with decreasing prestress, reaching its maximum, followed by decreases at smaller values for all nt-Cu. However, the critical prestress at the maximum indentation hardness significantly depends on twin spacing. Finally, a model was developed to explain this special deformation behavior. The present results could deepen our understanding of the deformation behavior of nt-Cu and provide a new paradigm for the design of this material under complex stress state.

**Keywords:** coherent twin boundary; molecular dynamics; dislocation; copper; nanoindentation

## 1. Introduction

Engineering coherent twin boundaries (CTBs), which are defined as the (111) mirror planes in a face-centered cubic structure at which the normal stacking sequence of (111) planes is reversed, are an attractive strategy for strengthening metallic materials while preserving their desired ductility [1]. When abundant CTBs with a nanoscale twin thickness (the spacing between two adjoining twin boundaries) are introduced into metallic materials (i.e., nanotwinned metals), some unprecedented properties such as ultra-high strength [2–5], high tensile ductility [2,3], considerable work hardening [6,7], and history-independent cyclic response [8] are achieved. Experiments and molecular dynamics (MD) simulations revealed that the novel mechanical properties of nanotwinned metals originate from the complicated effect of CTBs on the plastic deformation. Compared with conventional grain boundaries (GBs), CTBs not only effectively hinder dislocation motion and thus act as stable interfaces for strengthening metals [9–11], but also facilitate the storage of dislocations and thus accommodate plastic deformation [11]. Even so, many studies have reported that the introduction of CTBs into metallic materials could cause a hardening effect, weakening effect, or no

effect depending on the twin thickness, sample extrinsic size, and intrinsic size [12–16]. Some atomistic simulations suggested that CTBs have an unfavorable effect on ductility, and facilitate brittle fractures in nanowires [17,18]. Hence, the influence of CTBs on the plastic deformation of nanotwinned metals is not well understood, and the meticulous architecture of nanotwinned metals is urgently needed.

The nanoindentation has been developed into a high spatial resolution micro-probe means to measure mechanical properties at the microscale and nanoscale [19–21]. Typically, nanoindentation has been employed to evaluate the mechanical properties and deformation kinetic parameters of nanotwinned copper (nt-Cu) [22,23]. This is due to the advantages that this technique offers, such as its simple procedure, large strain range compared with the tensile test, and the requirement of only a small volume of material. During nanoindentation, the prestress or residual stress has a significant effect on the load-depth curve, and thus influences the hardness and modulus measurements [24,25]. Indeed, nanoindentation has been used to measure prestress in materials given its advantages of simplicity, non-destruction, applicability, and convenience at various scales [26,27]. Many empirical models have been developed to evaluate the prestress, and are well described in Zhu et al.'s review [28]. However, the plastic deformation mechanism depending on prestress, which involves considerable difficulty for use in experiments, is rarely seen. Fortunately, the MD simulation provides a very powerful approach to reveal the mechanical behavior and plasticity mechanism at the atomic scale. By using MD simulations, Schall et al. [29] accurately determined the true contact area during the plastic indentation of single crystal Au under an applied in-plane stress. They found that the mean pressure varied slightly with applied prestress with higher values in compression than in tension. Sun et al. [30,31] simulated the spherical nanoindentation of a single crystal copper thin film with in-plane residual stress. The result indicated that the residual stress not only significantly influenced the surface strength, but also gave rise to the transition of dislocation nucleation behavior. These studies notably made considerable progress in understanding the nanoindentation behavior of materials.

In nanotwinned metal, the pre-existing CTBs induce a special deformation behavior and mechanism, thus leading to a special response to prestress under nanoindentation, which could be very different from the defect-free metal in previous MD simulations [29–31]. In the present paper, we revealed the effect of equi-biaxial prestress and twin spacing on the mechanical response of nt-Cu under nanoindentation using the MD simulation. We paid special attention to the combined effect of pre-existing CTBs and prestress on the hardening-to-softening transition and plastic deformation mechanism at an atomic scale.

## 2. Methods

In this work, the MD simulations were performed using LAMMPS [32] with an embedded-atom method (EAM) potential for Cu [33]. The rectangular nt-Cu samples were created containing orthogonally oriented CTBs with the initial size of  $23.5 \times 23.5 \times 24.0 \text{ nm}^3$  and consisted of 1,121,480 atoms, as shown in Figure 1. A free boundary condition was applied along [111] orientation, which is just the indenting direction, while periodic boundary conditions were imposed along  $\bar{1}10$  and  $11\bar{2}$  orientation. The twin lamella length (denoted as  $\lambda$ ) was chosen to be 1.25 nm, 3.67 nm, and 5.64 nm.

The initial sample was relaxed under zero-pressure and 0.1 K for 50 ps. The equi-biaxial prestress ranging from  $-5 \text{ GPa}$  to  $4 \text{ GPa}$  was then gradually imposed along  $\bar{1}10$  and  $11\bar{2}$  orientation within 20 ps and followed by relaxation for 50 ps, while no stress was exerted along [111] orientation. In this processing, the calculation cell could be freely expanded or shrunk two-dimensionally to maintain the applied equi-biaxial prestress. Then, the sample was indented along the [111] orientation with a constant velocity of  $10 \text{ m/s}$ , in which the applied equi-biaxial prestress was maintained. The virtual spherical indenter with a radius  $R = 8 \text{ nm}$  was modeled using a repulsive force with a force constant of  $10 \text{ eV}/\text{\AA}^2$  [34]. The atoms in a layer with a thickness of  $1 \text{ nm}$  at the bottom were frozen to provide structural stability, while all other atoms were free moved under the canonical ensemble (NVT) at a fixed temperature of  $0.1 \text{ K}$ . The common neighbor analysis (CNA) [35] was used to identify the defects. The AtomEye software was used to visualize the atomic configurations [36].

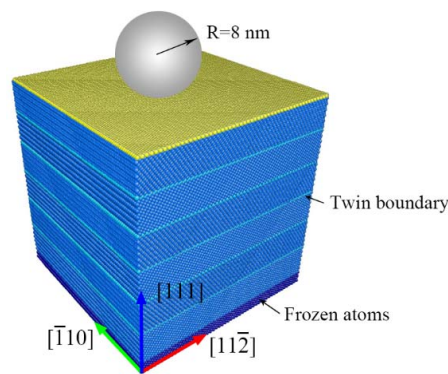


Figure 1. Molecular dynamics simulation model.

### 3. Results and Discussion

#### 3.1. Mechanical Behavior

We first evaluated the indentation hardness  $H$ , which is obtained from the critical load at which initial dislocation nucleates are divided by the projected contact area of atoms in direct contact. In our previous work [14], we revealed that  $H$  gradually increases with decreasing twin spacing, reaching a maximum at 3.60 nm, followed by a softening at smaller values. This shows a hardening-to-softening transition depending on twin spacing. The strongest twin spacing originates from a transition in the initial plasticity mechanism from the suppressive nucleation of partial dislocation to twin simulative nucleation of twinning partial [14]. Hence, three typical twin spacings of 1.25 nm, 3.67 nm, and 5.64 nm were chosen to elucidate the combined effect of the twin spacing and prestress.

Figure 2 shows the indentation hardness  $H$  as a function of the prestress  $\sigma_r$  for the nt-Cu and its single crystal counterpart (sc-Cu). As the prestress is free, the  $H$  of the nt-Cu with  $\lambda = 3.67$  nm is larger than that of the sc-Cu and nt-Cu with other twin spacings, indicating optimum strengthening capability. Notably, the hardening effect of the nt-Cu with  $\lambda = 3.67$  nm gradually degenerates when compressive prestress is imposed. Even softening arises when the compressive prestress is larger than 1 GPa, as shown in Figure 2a. In contrast, in the tensile prestress regime the hardening effect is maintained. When  $\lambda$  decreases to less than 3.67 nm, significant softening is observed regardless of the prestress, as indicated in Figure 2b. For example, the hardness of the nt-Cu with  $\lambda = 1.25$  nm decreases by 24.24% compared with sc-Cu when the prestress is free, while the maximum hardness increase is only 2.90% for the nt-Cu with  $\lambda = 3.67$  nm when the prestress is 1 GPa. In contrast, when  $\lambda$  is over 3.67 nm hardening is observed regardless of prestress (see Figure 2a).

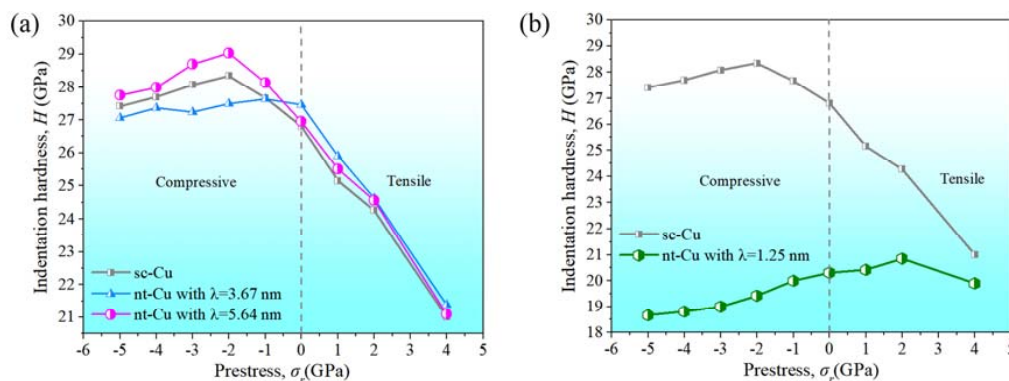


Figure 2. The indentation hardness as a function of the prestress for (a) single crystal copper (sc-Cu) and nanotwinned copper (nt-Cu) with large twin spacings and (b) sc-Cu and nt-Cu with small twin spacing. Positive values represent tensile stress while negative values indicate compressive stress.

All the nt-Cu and sc-Cu have a similar change of indentation hardness with the decreasing of prestress, i.e., indentation hardness firstly increases, reaches its maximum and then decreases, as illustrated in Figure 2. The critical prestress for the maximum indentation hardness of nt-Cu is strongly dependent on the twin spacing, which decreases from 2 GPa to  $-2$  GPa with the increase of twin spacing. This scenario is different from the experiment and finite element simulation results where the hardness monotonously decreases by increasing the prestress or residual stress [24].

The present result demonstrates that twin spacing and prestress have a complex mutual effect on the mechanical behavior of nt-Cu. Hardening-to-softening transition always occurs at any prestress with decreasing twin spacing in nt-Cu compared with its single crystal counterpart, while it occurs at a specific twin spacing of 3.67 nm with decreasing prestress. Softening is always observed with small twin spacings; the strengthening is observed with large twin spacings. Despite all this, we will state that the same mechanism controls the hardening-to-softening transition depending on twin spacing and prestress.

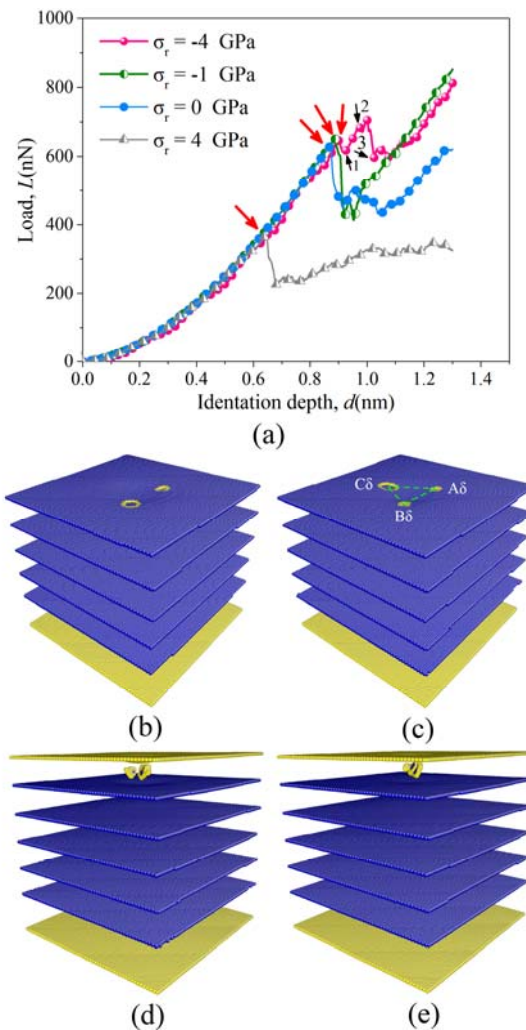
### 3.2. Deformation Mechanism at the Atomic Level

Figure 3 shows the initial dislocation activation and load-displacement curves in the nt-Cu with  $\lambda = 3.67$  nm and sc-Cu. A key interesting result is that the transition of initial load relaxation mechanism is observed with the change of prestress. When prestress is larger than  $-1$  GPa, the initial load relaxation, displayed as a discontinuity in load-displacement curves, is due to the subsurface, homogenous nucleation of the threefold symmetry dislocation embryos on  $\{111\}$  plane for the nt-Cu, as shown in Figure 3d,e. These dislocation embryos will expand into three partial dislocation loops as the indentation proceeds. Once prestress is less than  $-1$  GPa, the initial load relaxation is due to the homogenous nucleation of the threefold symmetry dislocation embryos on CTB (see Figure 3b,c). With the increase of applied load, these dislocation embryos expand into three twinning partial loops, which are off the indenter axis at an orientation of  $120^\circ$  with respect to each other. These twinning partial loops have the Burgers vectors of  $1/6[\bar{1}2\bar{1}]$  (A $\delta$ ),  $1/6[2\bar{1}\bar{1}]$  (B $\delta$ ), and  $1/6[\bar{1}\bar{1}2]$  (C $\delta$ ). The dislocation sourcing from CTBs has been reported in nt-Cu with small twin boundary spacing [14], and with the destroyed CTBs [37,38]. The present result indicates that the large compressive prestress state facilitates the dislocation sourcing from perfect CTBs, accompanying a reduction in indentation hardness. Hence, the hardening-to-softening transitions induced by decreasing either twin spacing or prestress are due to same mechanism, i.e., transition of initial plasticity mechanism from activation of partial dislocation to twinning dislocation.

For sc-Cu, the initial load relaxation is due to the homogenous nucleation of the threefold symmetry dislocation embryos in the subsurface, as shown in Figure 4. Interestingly, when prestress decreases to less than  $-2$  GPa, three partial embryos nucleate and extend along the distorted (111) plane, which further expand into three partial loops, as indicated in Figure 4b,c. Notably, these partials have the same Burgers vectors as the twinning partial in nt-Cu. The nt-Cu with  $\lambda = 5.64$  nm shows the same transition of deformation mechanism at the critical prestress of  $-2$  GPa as sc-Cu, but with a large indentation hardness. The nt-Cu with  $\lambda = 1.25$  nm shows the transition of the initial plasticity mechanism from the activation of partial dislocation to twinning dislocation at the critical prestress of 2 GPa with decreasing prestress. Above all, the present result showed that large prestress facilitates the activation of dislocation on (111) plane both in nt-Cu and sc-Cu, giving rise to the observed change of indentation hardness with prestress, as shown in Figure S1 in Supplementary Materials.

We noted that the initial dislocations nucleate and extend along the (111) plane for the sc-Cu and along CTB for the nt-Cu only induce small load relaxation, as shown in Figures 3a and 4a. In fact, these dislocations can limitedly extend along the (111) plane with the increase of applied load for the sc-Cu, as shown in Figure 5a. As indentation proceeded, the subsequent large load relaxation was mediated by the nucleation and expansion of glide loops on the  $\{111\}$  plane inclined to the indentation axial, as indicated in Figure 5b,c. This is just the case in sc-Cu with small prestress values with a small prestress.

For the nt-Cu with  $\lambda = 3.67$  nm at large  $\sigma_r = 4$  GPa, following the homogenous nucleation event, the sliding of twinning partial loops is immediately terminated when they intersect with each other, as indicated in Figure 5d. This dislocation event results in the development of the first small load relaxation. As the indentation proceeds, three threefold symmetry partials nucleate and expand into partial dislocation loops along the (111) plane between the CTB and surface, accompanied by the second small load relaxation (see Figure 5e). This dislocation event is similar to the one observed in the sc-Cu at high prestress. With the increase of applied load, the large load relaxation is found in the load-displacement curves, which is mediated by the nucleation and expansion of gliding loops along the {111} plane inclined to the indentation axial, as shown in Figure 5f.



**Figure 3.** Load-displacement curves (a) and corresponding atomistic snapshots of the nt-Cu with  $\lambda = 3.67$  nm and (b)  $\sigma_r = -4$  GPa; (c)  $\sigma_r = -1$  GPa, (d)  $\sigma_r = 0$  GPa; (e)  $\sigma_r = 4$  GPa. The red arrows denote the event of initial load relaxation. The atoms are colored according to common neighbor analysis (CNA), where atoms with perfect face-centered cube (fcc) lattices are hidden for clarity, and the atoms in the surface are hidden in (b) and (c).

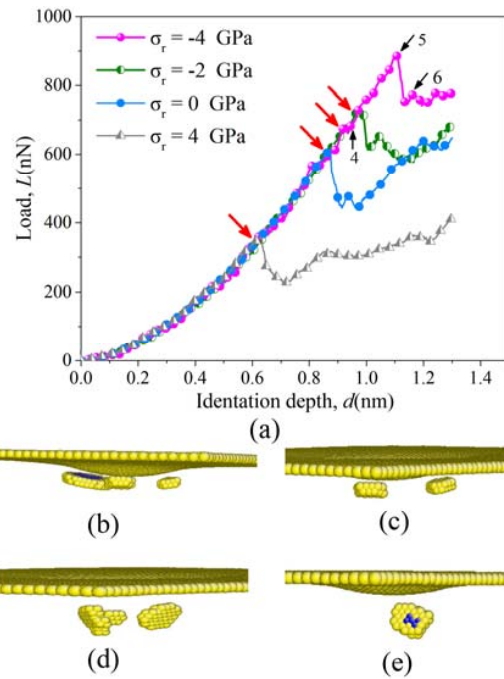


**Figure 4.** Load-displacement curves (a) and corresponding atomistic snapshots of the sc-Cu with (b)  $\sigma_r = -4$  GPa; (c)  $\sigma_r = -2$  GPa; (d)  $\sigma_r = 0$  GPa; (e)  $\sigma_r = 4$  GPa. The red arrows denote the event of initial load relaxation. The atoms are colored according to CNA, where atoms with perfect fcc lattices are hidden for clarity.

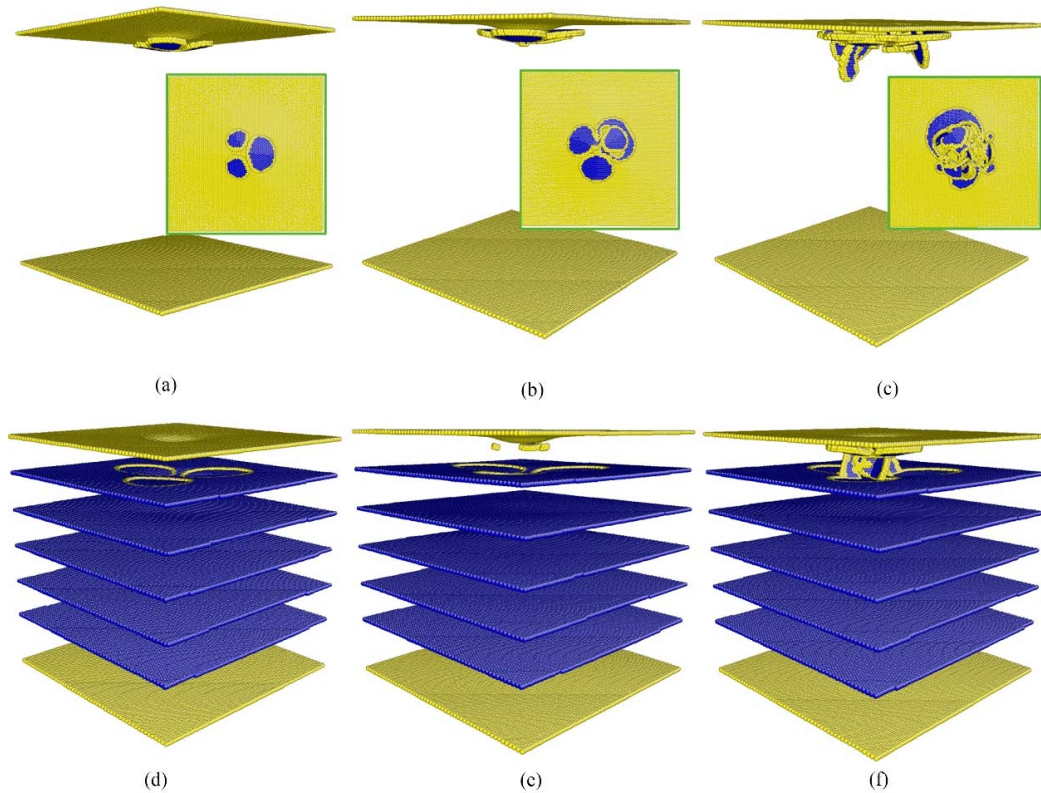


**Figure 5.** Atomistic snapshots of incipient plasticity of the sc-Cu at  $\sigma_r = 4$  GPa corresponding to the labeled points (a) 4; (b) 5; (c) 6 in Figure 4, and of the nt-Cu with  $\lambda = 3.67$  nm at  $\sigma_r = -4$  GPa corresponding to the labeled points (d) 1; (e) 2, (f) 3 in Figure 3.

The observed prestress- and twin spacing-dependent indentation hardness can be explained by using the elastic contact theory that comprehensively considers prestress and the two-phase model of Chen et al. [39]. According to the Hertz theory of elastic contact and Tresca yield criterion, the spherical indentation hardness  $H$  can be related to the yield stress  $\sigma_y$  and the critical shear stress  $\tau_{\text{cri}}$  at the onset of plastic deformation [40]:

$$H = 1.07\sigma_y = 2.14\tau_{\text{cri}} \quad (1)$$

Considering the equi-biaxial prestress and the Tresca yield criterion, the prestress is directly superimposed into the shear stress imposed by the indenter, and thus Equation (1) becomes:

$$H = 1.07(\sigma_y - \sigma_r) = 2.14\tau_{\text{cri}} - 1.07\sigma_r \quad (2)$$

As the first dislocation nucleates in the subsurface, a dislocation-CTB interaction force  $\tau_{\text{CTB}}$  due to the elasticity mismatch between the matrix and twin grains in terms of the shear modulus across the CTB, and a dislocation-surface interaction force  $\tau_{\text{surf}}$ , should be contributed to the critical resolved shear stress:

$$\tau_{\text{cri}} = \tau_0 + \tau_{\text{CTB}} + \tau_{\text{surf}} \quad (3)$$

where  $\tau_0$  is the theoretical shear strength, which can be regarded as constant. The dislocation tends to be repelled by CTB at large distances (i.e.,  $>3|b|$  where  $b$  is the Burgers vector) and is attracted by the surface. Hence,  $\tau_{\text{CTB}}$  is a repulsive force, and  $\tau_{\text{surf}}$  is an attractive force.

Considering a straight pure screw dislocation of infinite length,  $\tau_{\text{CTB}}$  is obtained according to the two-phase model of Chen et al. [39], as follows:

$$\tau_{\text{CTB}} = \frac{\alpha\mu b}{4\pi x_{\text{CTB}}} \sin \theta \quad (4)$$

where  $x_{\text{CTB}}$  is the distance between the CTB and dislocation nucleation site;  $\mu$  is the shear modulus along the slip system;  $\alpha$  is a dimensionless measure of the intrinsic strength due to the elasticity mismatch between the matrix and the twin, which is generally lower than 1 [39]; and  $\theta$  is the angle between the glide plane and the CTB, i.e., the dislocation nucleation angle.

The dislocation-surface interaction force  $\tau_{\text{CTB}}$  can be similarly written as:

$$\tau_{\text{surf}} = -\frac{\mu b}{4\pi x_{\text{surf}}} \sin \varphi \quad (5)$$

where  $x_{\text{surf}}$  is the distance between the surface and dislocation nucleation site, and  $\varphi$  is the angle between the glide plane and the surface.

Therefore, the indentation hardness  $H$  for nt-Cu can be obtained by substituting Equations (3)–(5) and Equation (2), as follows:

$$H^{\text{nt-Cu}} = 2.14 \left( \tau_0 + \frac{\alpha\mu b}{4\pi x_{\text{CTB}}} \sin \theta - \frac{\mu b}{4\pi x_{\text{surf}}} \sin \varphi \right) - 1.07\sigma_r \quad (6)$$

For sc-Cu, the  $\tau_{\text{CTB}}$  disappears. The indentation hardness  $H$  is given:

$$H^{\text{sc-Cu}} = 2.14 \left( \tau_0 - \frac{\mu b}{4\pi x_{\text{surf}}} \sin \varphi \right) - 1.07\sigma_r \quad (7)$$

We found that the nucleation sites are almost located at the same depth of 0.25 relative to the indenter radius for the nt-Cu and sc-Cu when the first dislocation nucleates on the {111} plane inclined to the indentation axial. Hence, the increased  $H$  for the nt-Cu (i.e., hardening effect) comes from the additional dislocation-CTB interaction force  $\tau_{\text{CTB}}$ . From Equations (6) and (7), it can be observed that the indentation hardness linearly decreases with prestress. The predicted linear dependence of  $H$ - $\sigma_r$  is

consistent with the MD simulation result when the initial partials propagate on the {111} plane inclined to the indentation axial. The observed hardness decrease with the decrease of prestress is obviously related to the dislocation-CTB interaction force  $\tau_{CTB}$  and dislocation-surface interaction force  $\tau_{surf}$ . Thus, the dislocation nucleation depth and angle are the key parameters. For the sc-Cu, Ma et al. [31] stated that the hardness decrease was due to the change of dislocation nucleation angle when the prestress decreased to a critical value. In fact, due to the large local deformation of surface during indenting, the dislocation nucleation depth and angle are difficult to determine. A detailed explanation for the deviation of linear dependence of  $H-\sigma_r$  still needs to be explored.

For the nt-Cu with  $\lambda = 1.25$  nm, the initial load relaxation is due to the homogenous nucleation of twin partials. The dislocation nucleation depth is approximately equal to twin spacing of 1.25 nm (0.16 relative to the indenter radius), which is much smaller than that for the sc-Cu and nt-Cu when first dislocation nucleates on the {111} plane inclined to indentation axial. It will lead to the increase of the dislocation-surface interaction force  $\tau_{surf}$ , and potentially lead to a decrease in hardness. Moreover, because the CTB provides additional energy for dislocation nucleation [41,42], the nucleation of twin partials is more favorable than partial dislocations in perfect crystal Cu. Therefore, nt-Cu with  $\lambda = 1.25$  nm exhibits significant softening regardless of the prestress, as shown in Figure 2b.

The present result suggests that the prestress can significantly influence the hardness of nt-Cu. Thus, meticulous processing should be employed to eliminate the prestress when nanoindentation is used to evaluate the mechanical behavior of nt-Cu, especially when the effect of twin spacing on mechanical behavior is investigated. Moreover, Equations (6) and (7) can be used to extract the prestress or residual stress when the nanoindentation is used. Notably, they are only valid when the compress prestress is small and the twin spacing is relatively large.

#### 4. Conclusions

In conclusion, prestress- and twin spacing-dependent deformation behavior and its mechanism were investigated using MD simulations at the atomic level. The result demonstrates that prestress and twin spacing have a complex mutual effect on the mechanical behavior of nt-Cu. The hardening-to-softening transition always occurs at any prestress with decreasing twin spacing in nt-Cu compared with its single crystal counterpart, while it occurs at a specific twin spacing with decreasing prestress. The softening is observed with small twin spacing; the strengthening is observed with large twin spacing. The same mechanism controls this hardening-to-softening transition induced by decreasing either the twin spacing or prestress, i.e., the transition in the initial plasticity mechanism from the activity of partial dislocation to twinning dislocation.

Similar changes in the indentation hardness with prestress is found in all nt-Cu and sc-Cu, i.e., indentation hardness increases with decreasing prestress, reaching its maximum, followed by decreases at smaller values. However, the critical prestress at the maximum indentation hardness significantly depends on twin spacing. The large prestress facilitates the activation of dislocation on the (111) plane both in both nt-Cu and sc-Cu, giving rise to the observed change in indentation hardness with prestress. Finally, a model considering the prestress, dislocation-surface interaction force, and dislocation-CTB interaction force was developed to explain this special deformation behavior.

**Supplementary Materials:** The following are available online at <http://www.mdpi.com/2075-4701/8/5/344/s1>, Figure S1: The indentation hardness as a function of the prestress for sc-Cu (a) and nt-Cu with  $\lambda = 3.67$  nm (b). The inserts show the atomistic snapshots at initial load relaxation.

**Author Contributions:** J.H. and J.S. designed the project, guided the research, and prepared the manuscript. J.H. and Y.H. performed the simulation. J.H. and J.S. analyzed the data and prepared the figures. L.F. and H.Z. reviewed the manuscript.

**Acknowledgments:** The authors acknowledge financial support received from the National Natural Science Foundation of China (Grant No. 51505479 and 51605139), the Natural Science Foundation of Jiangsu Province (Grant No. BK20150184 and BK20160867), the Fundamental Research Funds for the Central Universities (Grant No. 2015XKMS019), and the China Postdoctoral Science Foundation (Grant No. 2014M551686). We also

acknowledge the support of a project funded by the Priority Academic Program Development of Jiangsu Higher Education Institutions.

**Conflicts of Interest:** The authors declare no conflict of interest.

## References

1. Lu, K.; Lu, L.; Suresh, S. Strengthening materials by engineering coherent internal boundaries at the nanoscale. *Science* **2009**, *324*, 349–352. [[CrossRef](#)] [[PubMed](#)]
2. Lu, L.; Chen, X.; Huang, X.; Lu, K. Revealing the maximum strength in nanotwinned copper. *Science* **2009**, *323*, 607–610. [[CrossRef](#)] [[PubMed](#)]
3. Lu, L.; Shen, Y.F.; Chen, X.H.; Qian, L.H.; Lu, K. Ultrahigh strength and high electrical conductivity in copper. *Science* **2004**, *304*, 422–426. [[CrossRef](#)] [[PubMed](#)]
4. Jang, D.C.; Li, X.Y.; Gao, H.J.; Greer, J.R. Deformation mechanisms in nanotwinned metal nanopillars. *Nat. Nanotechnol.* **2012**, *7*, 594–601. [[CrossRef](#)] [[PubMed](#)]
5. Wang, J.; Sansoz, F.; Huang, J.; Liu, Y.; Sun, S.; Zhang, Z.; Mao, S.X. Near-ideal theoretical strength in gold nanowires containing angstrom scale twins. *Nat. Commun.* **2013**, *4*, 1742. [[CrossRef](#)] [[PubMed](#)]
6. Chen, X.H.; Lu, L. Work hardening of ultrafine-grained copper with nanoscale twins. *Scr. Mater.* **2007**, *57*, 133–136. [[CrossRef](#)]
7. Lu, L.; You, Z.S.; Lu, K. Work hardening of polycrystalline Cu with nanoscale twins. *Scr. Mater.* **2012**, *66*, 837–842. [[CrossRef](#)]
8. Pan, Q.; Zhou, H.; Lu, Q.; Gao, H.; Lu, L. History-independent cyclic response of nanotwinned metals. *Nature* **2017**, *551*, 214–221. [[CrossRef](#)] [[PubMed](#)]
9. Afanasyev, K.A.; Sansoz, F. Strengthening in gold nanopillars with nanoscale twins. *Nano Lett.* **2007**, *7*, 2056–2062. [[CrossRef](#)]
10. Deng, C.; Sansoz, F. Fundamental differences in the plasticity of periodically twinned nanowires in Au, Ag, Al, Cu, Pb and Ni. *Acta Mater.* **2009**, *57*, 6090–6101. [[CrossRef](#)]
11. Zhu, L.L.; Ruan, H.H.; Li, X.Y.; Dao, M.; Gao, H.J.; Lu, J. Modeling grain size dependent optimal twin spacing for achieving ultimate high strength and related high ductility in nanotwinned metals. *Acta Mater.* **2011**, *59*, 5544–5557. [[CrossRef](#)]
12. Deng, C.; Sansoz, F. Size-dependent yield stress in twinned gold nanowires mediated by site-specific surface dislocation emission. *Appl. Phys. Lett.* **2009**, *95*, 091914. [[CrossRef](#)]
13. Li, X.Y.; Wei, Y.J.; Lu, L.; Lu, K.; Gao, H.J. Dislocation nucleation governed softening and maximum strength in nano-twinned metals. *Nature* **2010**, *464*, 877–880. [[CrossRef](#)] [[PubMed](#)]
14. Sun, J.; Fang, L.; Sun, K.; Han, J. Direct observation of dislocations originating from perfect twin boundaries. *Scr. Mater.* **2011**, *65*, 501–504. [[CrossRef](#)]
15. Guo, X.; Xia, Y.Z. Repulsive force vs. Source number: Competing mechanisms in the yield of twinned gold nanowires of finite length. *Acta Mater.* **2011**, *59*, 2350–2357. [[CrossRef](#)]
16. Wei, Y. Anisotropic size effect in strength in coherent nanowires with tilted twins. *Phys. Rev. B* **2011**, *84*, 014107. [[CrossRef](#)]
17. Sun, J.; Li, C.; Han, J.; Shao, X.; Yang, X. Size effect and deformation mechanism in twinned copper nanowires. *Metals* **2017**, *7*, 438. [[CrossRef](#)]
18. Sun, J.; Fang, L.; Ma, A.; Jiang, J.; Han, Y.; Chen, H.; Han, J. The fracture behavior of twinned Cu nanowires: A molecular dynamics simulation. *Mater. Sci. Eng. A* **2015**, *634*, 86–90. [[CrossRef](#)]
19. Sun, J.; Cheng, L.; Han, J.; Ma, A.; Fang, L. Nanoindentation induced deformation and pop-in events in a silicon crystal: Molecular dynamics simulation and experiment. *Sci. Rep.* **2017**, *7*, 10282. [[CrossRef](#)] [[PubMed](#)]
20. Sebastiani, M.; Johanns, K.E.; Herbert, E.G.; Pharr, G.M. Measurement of fracture toughness by nanoindentation methods: Recent advances and future challenges. *Curr. Opin. Solid State Mater. Sci.* **2015**, *19*, 324–333. [[CrossRef](#)]
21. Oliver, W.C.; Pharr, G.M. Measurement of hardness and elastic modulus by instrumented indentation: Advances in understanding and refinements to methodology. *J. Mater. Res.* **2004**, *19*, 3–20. [[CrossRef](#)]
22. Liu, Y.; Hay, J.; Wang, H.; Zhang, X. A new method for reliable determination of strain-rate sensitivity of low-dimensional metallic materials by using nanoindentation. *Scr. Mater.* **2014**, *77*, 5–8. [[CrossRef](#)]

23. Choi, I.; Kim, Y.; Wang, Y.M.; Ramamurty, U.; Jang, J. Nanoindentation behavior of nanotwinned Cu: Influence of indenter angle on hardness, strain rate sensitivity and activation volume. *Acta Mater.* **2013**, *61*, 7313–7323. [[CrossRef](#)]
24. Pham, T.; Kim, S. Determination of equi-biaxial residual stress and plastic properties in structural steel using instrumented indentation. *Mater. Sci. Eng. A* **2017**, *688*, 352–363. [[CrossRef](#)]
25. Suresh, S.; Giannakopoulos, A.E. A new method for estimating residual stresses by instrumented sharp indentation. *Acta Mater.* **1998**, *46*, 5755–5767. [[CrossRef](#)]
26. Huber, N.; Heerens, J. On the effect of a general residual stress state on indentation and hardness testing. *Acta Mater.* **2008**, *56*, 6205–6213. [[CrossRef](#)]
27. Lee, Y.H.; Kwon, D. Estimation of biaxial surface stress by instrumented indentation with sharp indenters. *Acta Mater.* **2004**, *52*, 1555–1563. [[CrossRef](#)]
28. Zhu, L.; Xu, B.; Wang, H.; Wang, C. Measurement of residual stresses using nanoindentation method. *Crit. Rev. Solid State* **2015**, *40*, 77–89. [[CrossRef](#)]
29. Schall, J.D.; Brenner, D.W. Atomistic simulation of the influence of pre-existing stress on the interpretation of nanoindentation data. *J. Mater. Res.* **2004**, *19*, 3172–3180. [[CrossRef](#)]
30. Sun, K.; Shi, J.; Ma, L. Atomistic Insights into the Effects of Residual Stress during Nanoindentation. *Crystals* **2017**, *7*, 240. [[CrossRef](#)]
31. Sun, K.; Shen, W.; Ma, L. The influence of residual stress on incipient plasticity in single-crystal copper thin film under nanoindentation. *Comput. Mater. Sci.* **2014**, *81*, 226–232. [[CrossRef](#)]
32. Plimpton, S. Fast parallel algorithms for short-range molecular-dynamics. *J. Comput. Phys.* **1995**, *117*, 1–19. [[CrossRef](#)]
33. Mishin, Y.; Mehl, M.J.; Papaconstantopoulos, D.A.; Voter, A.F.; Kress, J.D. Structural stability and lattice defects in copper: Ab initio, tight-binding, and embedded-atom calculations. *Phys. Rev. B* **2001**, *63*, 224106. [[CrossRef](#)]
34. Ziegenhain, G.; Hartmaier, A.; Urbassek, H.M. Pair vs many-body potentials: Influence on elastic and plastic behavior in nanoindentation of fcc metals. *J. Mech. Phys. Solids* **2009**, *57*, 1514–1526. [[CrossRef](#)]
35. Tsuzuki, H.; Branicio, P.S.; Rino, J.P. Structural characterization of deformed crystals by analysis of common atomic neighborhood. *Comput. Phys. Commun.* **2007**, *177*, 518–523. [[CrossRef](#)]
36. Li, J. AtomEye: An efficient atomistic configuration viewer. *Model. Simul. Mater. Sci.* **2003**, *11*, 173–177. [[CrossRef](#)]
37. Stukowski, A.; Albe, K.; Farkas, D. Nanotwinned fcc metals: Strengthening versus softening mechanisms. *Phys. Rev. B* **2010**, *82*, 224103. [[CrossRef](#)]
38. Wang, Y.M.; Sansoz, F.; Lagrange, T.; Ott, R.T.; Marian, J.; Barbee, T.W., Jr.; Hamza, A.V. Defective twin boundaries in nanotwinned metals. *Nat. Mater.* **2013**, *12*, 697–702. [[CrossRef](#)] [[PubMed](#)]
39. Chen, Z.M.; Jin, Z.H.; Gao, H.J. Repulsive force between screw dislocation and coherent twin boundary in aluminum and copper. *Phys. Rev. B* **2007**, *75*. [[CrossRef](#)]
40. Tabor, D. *The Hardness of Metals*; Clarendon Press: Oxford, UK, 1952.
41. Jin, Z.H.; Gumbsch, P.; Ma, E.; Albe, K.; Lu, K.; Hahn, H.; Gleiter, H. The interaction mechanism of screw dislocations with coherent twin boundaries in different face-centred cubic metals. *Scr. Mater.* **2006**, *54*, 1163–1168. [[CrossRef](#)]
42. Frøseth, A.; Van Swygenhoven, H.; Derlet, P.M. The influence of twins on the mechanical properties of nc-Al. *Acta Mater.* **2004**, *52*, 2259–2268. [[CrossRef](#)]

